

Article

Effect of Calcium Silicate and β -Tricalcium Phosphate Reinforcement on the Mechanical–Biological Properties of Freeze-Dried Collagen Composite Scaffolds for Bone Tissue Engineering Applications

Temesgen Yiber Anmut¹, Henni Setia Ningsih² , Hsueh-Huan Shih¹, Meng-Huang Wu^{3,4,5,6,*} 
and Shao-Ju Shih^{1,2,*} 

- ¹ Department of Materials Science and Engineering, National Taiwan University of Science and Technology, No. 43, Sec. 4, Keelung Road, Taipei 10607, Taiwan
- ² Department of Fragrance and Cosmetic Science, Kaohsiung Medical University, No. 100, Shih-Chuan 1st Road, Kaohsiung 80708, Taiwan
- ³ Department of Orthopedics, Taipei Medical University Hospital, Taipei 11031, Taiwan
- ⁴ Department of Orthopaedics, School of Medicine, College of Medicine, Taipei Medical University, Taipei 11031, Taiwan
- ⁵ Prospective Innovation Center, Taipei Medical University Hospital, Taipei 11031, Taiwan
- ⁶ TMU Biodesign Center, Taipei Medical University, Taipei 11031, Taiwan
- * Correspondence: maxwutmu@gmail.com (M.-H.W.); shao-ju.shih@mail.ntust.edu.tw (S.-J.S.); Tel.: +886-970405299 (M.-H.W.); +886-2-27303716 (S.-J.S.)

Abstract: The development of a collagen-based composite scaffold to repair damaged bone is one of many important issues in tissue engineering. In this study, pure collagen, collagen/ β -tricalcium phosphate (β -TCP), collagen/calcium silicate (CS), and collagen/ β -TCP/CS scaffolds were fabricated using the freeze-drying method. The phase compositions, microstructures, and mechanical properties were characterized using X-ray diffraction, scanning electron microscopy, and a universal testing machine, respectively. In addition, cell viability was evaluated using an MTT assay. Finally, the correlations between the density, mechanical properties, and biodegradation behaviors of pore size distributions were discussed.

Keywords: β -tricalcium phosphate; calcium silicate; collagen; freeze-drying scaffolds



Citation: Anmut, T.Y.; Ningsih, H.S.; Shih, H.-H.; Wu, M.-H.; Shih, S.-J. Effect of Calcium Silicate and β -Tricalcium Phosphate Reinforcement on the Mechanical–Biological Properties of Freeze-Dried Collagen Composite Scaffolds for Bone Tissue Engineering Applications. *Ceramics* **2023**, *6*, 548–560. <https://doi.org/10.3390/ceramics6010033>

Academic Editor: Gilbert Fantozzi

Received: 17 December 2022

Revised: 13 February 2023

Accepted: 15 February 2023

Published: 18 February 2023



Copyright: © 2023 by the authors. Licensee MDPI, Basel, Switzerland. This article is an open access article distributed under the terms and conditions of the Creative Commons Attribution (CC BY) license (<https://creativecommons.org/licenses/by/4.0/>).

1. Introduction

Although allografts and autografts have been clinically used worldwide for repairing and replacing fractured bones, their obtainable quantity is limited [1]. Furthermore, additional invasive surgical procedures involve risks of morbidity of the donor site [2,3], infection [4], and hypersensitivity [5]. To minimize these risks, researchers have focused on developing synthetic grafts to replace allografts and autografts, which contain three important components: scaffolds, growth factors, and progenitor cells [6]. The materials for scaffolds require porous structures for differentiating and regenerating tissues, among which polymers serve as potential candidates [7–9]. In recent years, scaffolds based on natural polymers, such as collagen, chitosan, gelatin, and silk, have been developed [10–12]. Among all the natural polymers, collagen is preferred, owing to its biocompatibility, biodegradability, and ability to promote cell adhesion on its surface [13–15]. However, collagen has the disadvantages of low mechanical strength (~0.1 GPa) compared to that of bone (~2–50 GPa) and a rapid biodegradation rate (4–5 weeks) [16–18]. To overcome the above disadvantages, collagen has been combined with various bioceramics to form composite scaffolds [19], whereas the common bioceramics for tissue engineering are β -tricalcium phosphate (β -TCP) [20] and calcium silicate (CS) [21]. Firstly, β -TCP provides superior biological properties due to its biodegradability, osteoconductivity, and

biocompatibility [22,23]. For example, Goodarzi et al. reported the compressive strain of the collagen/ β -TCP composite scaffold was 18% higher than that of the pure collagen scaffold [24], improving the mechanical property significantly. Furthermore, Zou et al. found that the new bone from a rabbit replaced the implanted collagen/ β -TCP composite scaffold after 12 weeks [25]. Secondly, CS silica-based bioceramics have excellent bioactivity. For instance, Wang et al. [26] and Dong et al. [27] both observed the formation of apatite on their CS/collagen scaffolds after immersion in the simulated body fluid. Thus, the addition of β -TCP and CS powders into collagen scaffolds could provide the advantages of improved mechanical properties, a slower degradation rate, and bioactivity.

Some techniques have been developed to prepare collagen scaffolds, such as solvent casting [28], electrospinning [29], and phase-separation [30]. Although solvent casting is a simple method for synthesizing a collagen scaffold, the residual organic solvent within the final product could be toxic to cells [31]. Meanwhile, electrospinning and phase-separation showed the drawbacks of small pore size ($\sim 10\ \mu\text{m}$), non-uniform distribution and complexity [30,32]. In contrast, the freeze-drying method provides the merits of non-toxicity, simplicity, and controllable pore size, which could overcome the above drawbacks [33].

Therefore, in this study, we aimed to fabricate pure collagen scaffolds, collagen/ β -TCP, collagen/CS, and collagen/ β -TCP/CS composite scaffolds via a freeze-drying technique. Furthermore, the phase compositions, morphologies, and mechanical properties were characterized using X-ray diffraction (XRD), scanning electron microscopy (SEM), and a universal testing machine, whereas density and biodegradability were evaluated by immersion tests. Finally, *in vitro* cell viability was assessed by MTT assay on osteoblast-like cells (MC3T3-E1).

2. Materials and Methods

2.1. Preparation of CS Powder

In this work, the spray drying technique was used for the preparation of CS powder with a molar ratio Ca:Si = 1:1. To start with, 80.89 g tetraethyl orthosilicate ($\text{Si}(\text{OC}_2\text{H}_5)_4$, 99.9%, Showa, Japan) was hydrolyzed in 1000 mL of deionized (DI) water by adding 1.3 mL of 1 M of hydrochloric acid (HCl, 35.0~37.0%, Honeywell, Charlotte, NC, USA) as the hydrolysis catalyst. After 2 h of stirring, 34.50 g of calcium nitrate tetrahydrate ($\text{Ca}(\text{NO}_3)_2 \cdot 4\text{H}_2\text{O}$, 98.5%, Showa, Gyoda, Japan) was added and stirred for another 24 h at 200 rpm to form the precursor solution. Next, the solution was directed into a spray dryer (SDDO-03, IDTA Machinery Co., Ltd., New Taipei City, Taiwan) set to 200 °C with a flow rate of 50 mL/min. The obtained spray-dried powders were collected and calcined a conventional furnace for an additional 1 h in at temperature of 600 °C with a heating rate of 5 °C/min.

2.2. Fabrication of Pure Collagen and Composite Scaffold

The pure collagen and composite scaffolds were fabricated via freeze-drying. Initially, the collagen was extracted from porcine tendons with purity of up to >95% (Horien Biochemical Technology Co., Ltd., Taiwan). For the pure collagen scaffold, the initial solutions were prepared by dissolving 2 wt% of collagens in DI water at room temperature and then stirring for 24 h. For the composite scaffolds, the initial slurries were prepared by adding commercial β -TCP (OsteoceraTM, Wiltron Co., Ltd., Taiwan), CS, or β -TCP/CS powders to the collagen. Next, for the freeze-drying process, the milky white slurry was then transferred into a square mold (10 × 10 × 10 mm) and frozen at $-45\ ^\circ\text{C}$ for 3 h with a pressure of <400 mTorr, and then heated to room temperature with a low pressure of <10 mTorr. Another freeze–thaw cycle was carried out (72 h at $-2\ ^\circ\text{C}$, and 16 h at $25\ ^\circ\text{C}$). The samples were further frozen at $-80\ ^\circ\text{C}$ for 48 h, and then lyophilized with a freeze dryer (FDS5B, BioTek, Germany) to form porous scaffold. Finally, the scaffolds were cross-linked using dehydrothermal treatment at 110 °C for 24 h under vacuum conditions [34], and were sterilized by γ -radiation with doses of 25–30 kGy. Finally,

three composite scaffolds of collagen/ β -TCP(10/90 wt%), collagen/CS (10/90 wt%), and collagen/ β -TCP/CS (10.0/67.5/22.5 wt%) were fabricated.

2.3. Characterization

First, the phase compositions of pure scaffolds, collagen collagen/ β -TCP, collagen/CS, and collagen/ β -TCP/CS composite scaffolds were examined using X-ray diffraction (XRD) with an X-ray diffractometer (D2 Phaser, Bruker, Ettlingen, Germany) equipped with Cu-K α monochromatic radiation with diffraction angles 2θ from 20° to 80° . In addition, the surface morphologies of both pure and composite scaffolds were observed using a field-emission scanning electron microscope (JSM 6500F, JEOL, Tokyo, Japan) at an accelerating voltage of 15 kV, with a working distance of 10 mm, using a secondary electron detector. The samples were prepared by freshly cutting the scaffold into small pieces. Then, carbon tape was used to attach the sample to SEM stubs. Note that the scaffolds were coated with platinum using a sputter coater (E-1030, Hitachi, Tokyo, Japan) before observation. In addition, the pore size was calculated using Image J 1.50i software. More than 100 pores were counted for each composition; for the pore size measurement, large and small pores were randomly chosen to calculate the average pore size and the standard deviation.

2.4. Density Test

The bulk densities (g/cm^3) of all scaffolds were calculated based on Archimedes' principle using the following equation:

$$\rho = M/V \quad (1)$$

where M denotes the mass and V denotes the volume of the scaffolds. Each determination was obtained by averaging the results of three measurements.

2.5. Mechanical Properties

The mechanical properties of both pure and composite scaffolds were measured using the universal testing machine (QC513PC, Yang-Yi, Tainan City, Taiwan). All scaffolds were divided into cuboidal shapes with the dimensions of $1 \times 1 \times 1$ cm. Three distinct samples were examined for each scaffold, and the stress and strain diagrams were used to measure the acquired compressive modulus values, which were calculated from the slope of linear of 10% strain. Note that 10% strain is within the common linear elastic region of compression stress–strain curve for scaffold materials (e.g., PHBV scaffold [35], and chitosan/bioactive glass scaffold [36]).

2.6. In Vitro Biodegradation

Following the standard protocol of ISO 10993-14, the biodegradability of the pure collagen scaffold, and collagen/ β -TCP, collagen/CS, and collagen/ β -TCP/CS composite scaffolds were examined by immersion in the citric acid solution. The specimens $1 \times 1 \times 1$ cm in size were soaked in 5 mL citric acid solution. The pH of the solution was controlled at 3, and the temperature was maintained at 37°C for 7 days. For the in vitro biodegradation tests, the seven scaffolds for each composition were characterized for seven time periods (days 1, 2, 3, 4, 5, 6, and 7). After biodegradation periods, the scaffolds were taken out from the citric acid solution and washed using DI water in order to remove the absorbed ion. Finally, the scaffolds were dried in the oven at 70°C for 24 h. Note that the solutions were replaced with fresh citric acid solution (pH 3) every day. The biodegradability of the composite scaffolds was computed with the following equation.

$$\text{Degradation rate (\%)} = \frac{W_0 - W_t}{W_0} \times 100 \quad (2)$$

where W_0 and W_t represent the initial weight and the incubated weight of the scaffold, respectively.

2.7. In Vitro Cytotoxicity

Finally, evaluation of cytotoxicity was examined via MTT assay. The mouse osteoblast cell line (MC3T3-E1, ATCC CRL-2594, Virginia, USA) was used to perform the assay for all scaffolds. First, the MC3T3-E1 cells were cultured in minimum essential medium- α (MEM- α , Gibco, Waltham, MA, USA) which contains 10% fetal bovine serum (FBS, Gibco, Waltham, MA, USA) and 1% penicillin-streptomycin (Thermo Fisher, Waltham, MA, USA). The cells were seeded onto 24 well plates, at a density of 2×10^4 cells/mL. The scaffolds (1 cm \times 1 cm \times 1 cm) were immersed in separate sterile tubes with 5 mL MEM- α and incubated at 37 °C for 24 h. To examine the cytotoxicity of the extractions, 4 mL of extraction was added to each well. After 3 d of incubation, 200 μ L of each MTT solutions was added and incubated for 4 h at 37 °C in an incubator with 95% humidity and 5% CO₂. Dimethyl sulfoxide (DMSO, Fisher Chemical, Fair Lawn, NJ, USA) was used to dissolve the crystal formazan, and the optical density (OD) at 570 nm was measured using the microplate reader (Multiskan Go, Thermo Scientific, Waltham, MA, USA). The percentage of cell viability in each scaffold was calculated against the control group. The statistical analysis was conducted to assess significant difference using *t*-test analysis, with the level of significance set to a *p* value of less than 0.05.

3. Results

The phase compositions of both pure and composite collagen scaffolds were examined using XRD, as the results are shown in Figure 1. Initially, the XRD pattern of the pure collagen scaffold showed a characteristic hump from 25° to 40°, which reveals the amorphous structure of collagen. Then, for the composite scaffolds, a single phase of β -TCP (JCPDS 09-0169) could be observed for the collagen/ β -TCP composite scaffold, while the collagen/CS composite scaffold showed a single phase of CS (JCPDS 33-0303). Lastly, the XRD pattern of collagen/ β -TCP/CS composite scaffold showed a major phase of β -TCP (JCPDS number of 09-0169) and a minor phase of CS (JCPDS number of 33-0303). Additionally, from XRD patterns, the characteristic hump of collagen was not obvious for the composite scaffolds of collagen/ β -TCP, collagen/CS, and collagen/ β -TCP/CS, which may have been due to the existence of crystalline β -TCP or CS particles. In brief, the XRD results indicated that the pure collagen scaffold exhibits the amorphous phase, whereas both crystalline phases of β -TCP and CS could be predicted for the composite scaffolds.

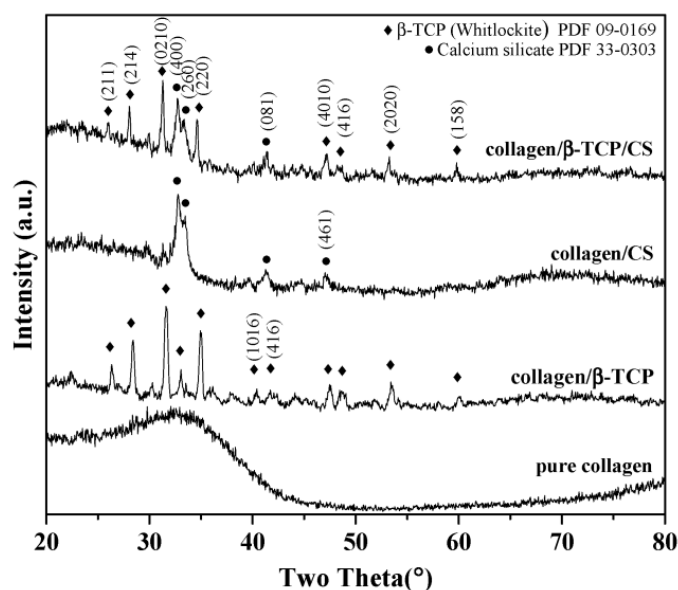


Figure 1. XRD patterns of pure collagen scaffold and collagen/ β -TCP, collagen/CS, and collagen/ β -TCP/CS composite scaffolds.

Figure 2 shows the shapes of both pure and composite collagen scaffolds. For the scaffold dimension, all photographs showed cubic shapes with nominal sizes of $10 \times 10 \times 10$ mm. In addition, for the surface roughness, a smooth surface was observed from the pure collagen scaffold (Figure 2a), and the surfaces of collagen/ β -TCP, collagen/CS, and collagen/ β -TCP/CS composite scaffolds revealed rougher morphologies as shown in Figure 2b–d. The results suggest that the roughness of scaffold surface increases with the adding of bioceramic particles (e.g., β -TCP or CS).

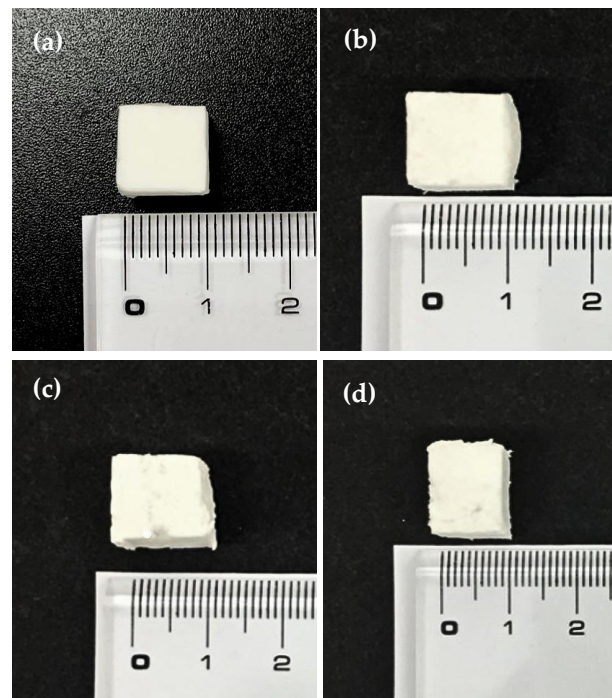


Figure 2. Photographs of (a) pure collagen scaffold, (b) collagen/ β -TCP, (c) collagen/CS, and (d) collagen/ β -TCP/CS composite scaffolds.

For the observation of microscopic structure, SEM was employed and the corresponding images are shown in Figure 3. Firstly, Figure 3a showed that the pure collagen scaffold has an interconnected porous structure, which is the typical structure after a freeze-drying process [37]. Meanwhile, similar porous structures could be observed for collagen/ β -TCP, collagen/CS, and collagen/ β -TCP/CS composite scaffolds, as shown in Figure 3b–d. In addition, the averaged pore sizes of collagen scaffold collagen/ β -TCP, collagen/CS, and collagen/ β -TCP/CS composite scaffolds were 81.00 ± 3.22 μm , 64.63 ± 18.96 , 45.07 ± 4.36 , and 26.53 ± 6.89 μm , respectively, showing the order of pore size was pure collagen > collagen/ β -TCP > collagen/CS > collagen/ β -TCP/CS. Furthermore, the results indicated that the β -TCP and CS particles decreased the average pore size of the collagen-based scaffold. For the collagen/ β -TCP composite scaffolds, the presence of β -TCP particles with the diameter of ~ 300 μm in the collagen/ β -TCP scaffolds are shown in Figure 3b. Meanwhile, ~ 10 μm CS particles could be observed in the collagen/CS and collagen/ β -TCP/CS composited scaffolds, as shown in Figure 3c,d. Additionally, from these SEM images, the commercial β -TCP particles and spray dried CS particles reveal the irregular and spherical shapes, respectively. In brief, the SEM results indicate the successful synthesis of porous collagen scaffolds with pure and collagen/ β -TCP, collagen/CS, and collagen/ β -TCP/CS composites.

Figure 4 reveals the densities of both pure and composite collagen scaffolds. The results show that the density of the pure collagen scaffold and collagen/ β -TCP, collagen/CS, and collagen/ β -TCP/CS composite scaffolds were 0.028 ± 0.002 , 0.534 ± 0.076 , 0.738 ± 0.027 , and 0.692 ± 0.007 g/cm^3 , respectively. This showed the order of density was collagen/ β -

TCP/CS > collagen/CS > collagen/ β -TCP > pure collagen, indicating that with the addition of β -TCP and CS powders, the density could be increased significantly from ~ 0.03 to ~ 0.70 .

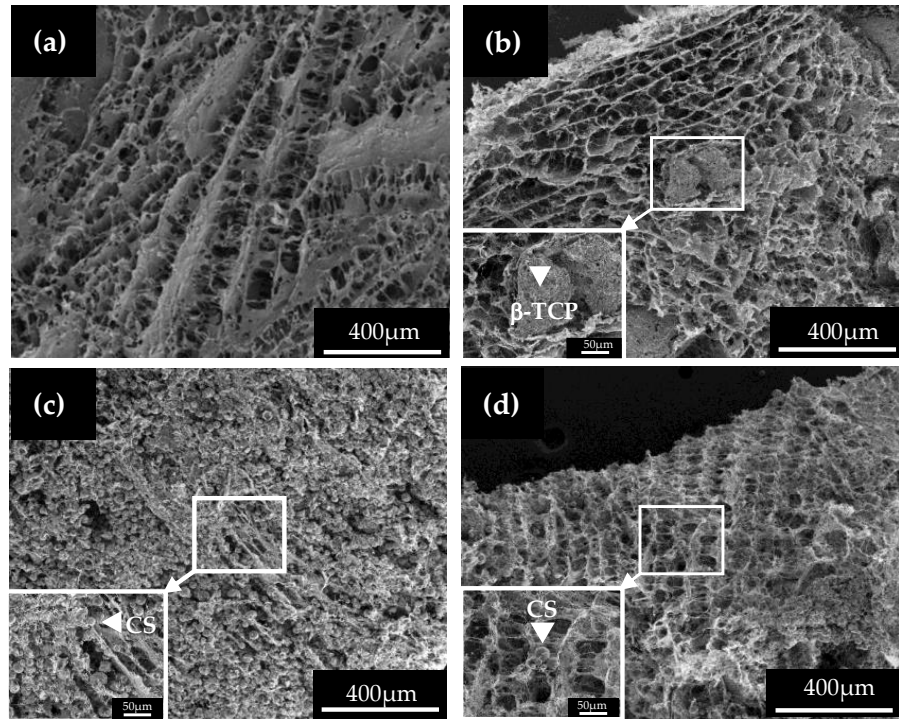


Figure 3. SEM images of (a) pure collagen scaffold, (b) collagen/ β -TCP, (c) collagen/CS, and (d) collagen/ β -TCP/CS composite scaffolds.

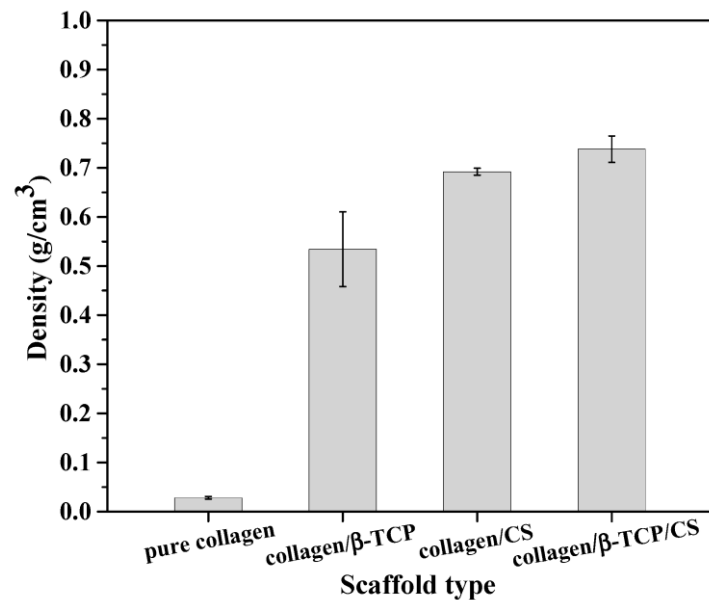


Figure 4. The densities of pure collagen scaffold and collagen/ β -TCP, collagen/CS, and collagen/ β -TCP/CS composite scaffolds.

The mechanical properties of pure collagen scaffold and composite scaffolds were measured using a compression test. Figure 5 shows the obtained stress–strain curves and the corresponding compressive modulus diagram. As shown in Figure 5a, all collagen scaffolds remained stable when subjected to up to 80% strain. In addition, a maximum stress of 0.61 MPa was observed for the collagen/CS specimen, followed by 0.30 MPa

for the collagen/ β -TCP/CS specimen, 0.27 MPa for the collagen/ β -TCP specimen, and 0.06 MPa for the pure collagen scaffold under the 80% strain condition. Furthermore, the compressive moduli of the pure collagen scaffold and composite scaffolds, as shown in Figure 5b, were computed from the condition of 10% strain due to the linear slopes of the stress–strain curves, and the results show that the compressive moduli for the pure collagen, collagen/ β -TCP, collagen/CS, and collagen/ β -TCP/CS composite scaffolds were 0.08, 1.58, 3.68, and 1.96 MPa, respectively. As compared to the pure collagen scaffold, the compressive moduli of the collagen/ β -TCP, collagen/CS, and collagen/ β -TCP/CS composite scaffolds were improved by 18.8, 45.0, and 23.5%, respectively. In summary, the increase in compressive modulus could be observed with the addition of CS particles.

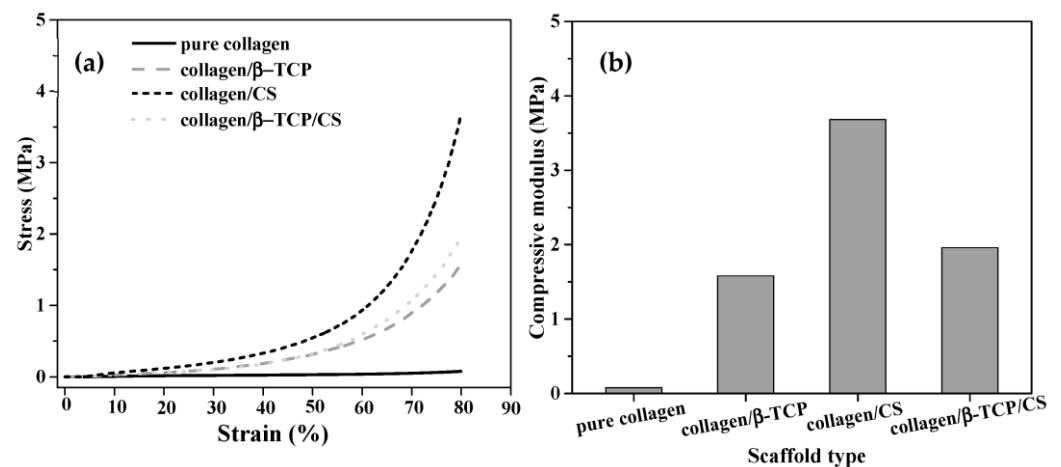


Figure 5. (a) Compressive stress–strain curve and (b) compressive modulus of pure collagen scaffold and collagen/ β -TCP, collagen/CS, and collagen/ β -TCP/CS composite scaffolds.

For the *in vitro* biodegradation test, the pure collagen scaffold and composite scaffolds were immersed in a citric acid solution (pH of 3) at 37 °C in a shaking incubator, following the international standard ISO 10993-14 [38]. Figure 6 shows the degradation behavior of both pure and composite collagen scaffolds. It can be seen in the figure that a weight loss of 86.5% was measured from the pure collagen scaffold after the first day of immersion. Subsequently, the degradation rate decreased, and the weight losses were 96.7%, 95.9%, and 98.9% at the periods of 2, 3, and 4 d, respectively. Finally, after 5 d of immersion, the pure collagen scaffold was completely degraded (100% weight loss). Next, a similar trend could be observed for the collagen/ β -TCP scaffold with a weight loss of 50.9% for the first day, then weight losses of 56.0%, 58.2%, 60.9%, 62.9%, 66.9%, and 69.3% for the 2, 3, 4, 5, 6, and 7 d immersion, respectively. In addition, unlike the pure collagen and collagen/ β -TCP scaffolds, the weight losses slightly increased for both the collagen/CS and collagen/ β -TCP/CS composite scaffolds; the weight losses of the collagen/CS scaffold are 2.4% for 1 d and 17.9% for 7 d, and the weight losses of the collagen/ β -TCP/CS are 5.7% for 1 d and 22.9% for 7 d. In short, the results showed that the order of weight loss of all scaffolds was pure collagen > collagen/ β -TCP > collagen/CS > collagen/ β -TCP/CS. Meanwhile, scaffolds with the addition of CS had much slower degradation rates than the other scaffolds (i.e., pure collagen and collagen/ β -TCP ones).

Finally, MTT assays were performed to determine the cell viability of all collagen scaffolds on osteoblast MC3T3-E1 cells, and the results are shown in Figure 7. Based on the graph, it can be observed that the cell viability of pure collagen scaffold and collagen/ β -TCP, collagen/CS, and collagen/ β -TCP/CS composite scaffolds were 101.50 ± 3.64 , 96.85 ± 5.81 , 89.71 ± 11.02 , and $83.82 \pm 13.58\%$, respectively. Additionally, the statistical analysis showed that the *p* values of collagen/ β -TCP, collagen/CS, and collagen/ β -TCP/CS composite scaffolds compared to pure collagen were 0.099, 0.334, and 0.161, respectively, which suggests that there was no significant difference in cell viability between the pure collagen

scaffold and composite scaffolds. In brief, these results demonstrate that both pure and composite collagen scaffolds showed cell viability higher than 70%, which indicates that there was no cytotoxic effect against MC3T3-E1 cells.

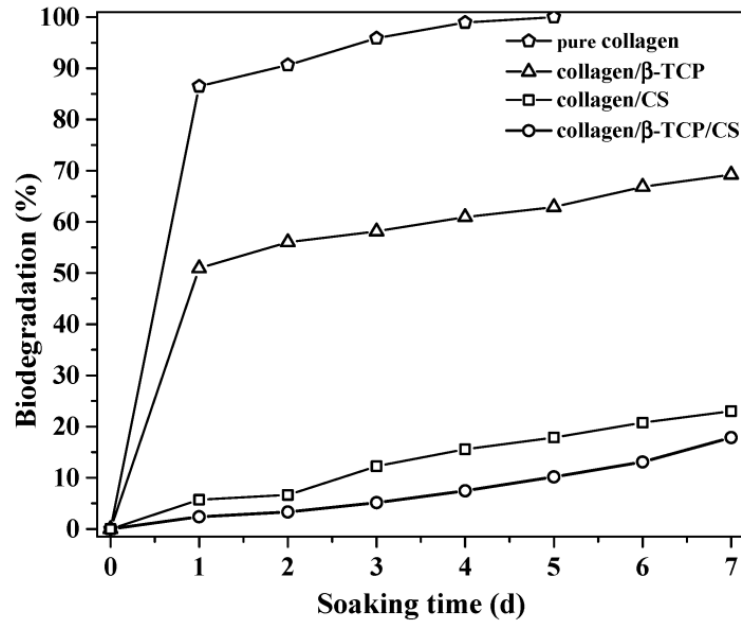


Figure 6. In vitro biodegradation of the pure collagen scaffold and collagen/β-TCP, collagen/CS, and collagen/β-TCP/CS composite scaffolds after soaking in citric acid solution for 7 d.

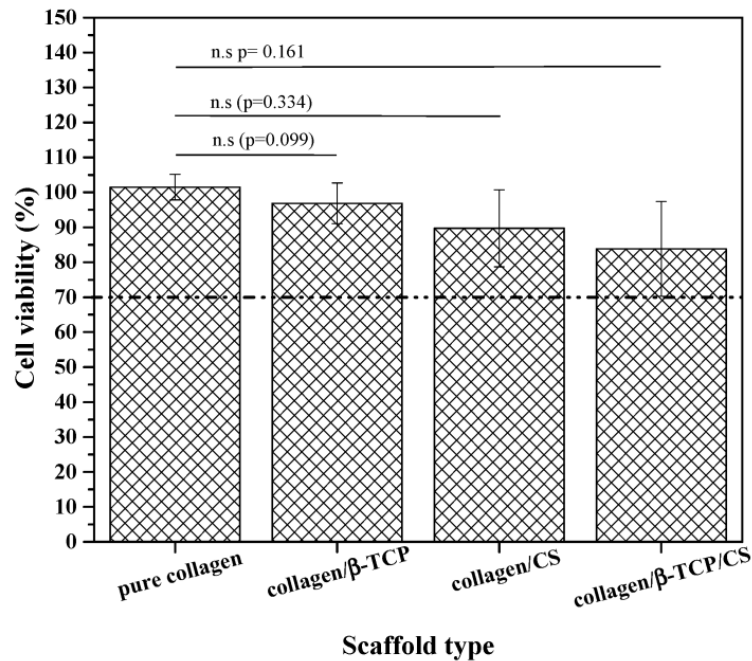


Figure 7. Cell viability of pure collagen scaffold and collagen/β-TCP, collagen/CS, and collagen/β-TCP/CS composite scaffolds derived from MC3T3-E1 cells after incubation for 3 d. n.s: not significant ($p > 0.05$).

4. Discussion

For the CS morphology, the SEM images (Figure 3c,d) revealed spherical particles, which is the typical spray-dried shape. In the spray-drying technique, powder morphology is determined by the factors of precursor properties and process condition (e.g., heating

temperature), and these factors are strongly related to the dimensionless Peclet (Pe) number, which is defined as the ratio of the solvent evaporation rate to the solute diffusion coefficient [39]. From the definition of Pe, a lower Pe number indicates the solvent's evaporation rate is slower than the solute's diffusional motion during the evaporation step; thus, the spherical morphology is observed. On the other hand, a higher Pe number shows a faster evaporation rate than the solute's diffusion motion, and an irregular morphology is obtained in this case. In this study, the sphere CS is attributed to a lower Pe number, similar to our previous study of spray-dried BG [40].

The phase composition and pore structure of all scaffolds are discussed below. For the phase composition, the XRD patterns confirmed the absence of any impurity phase, which indicated that all composite scaffolds were successfully synthesized using freeze-drying. Meanwhile, for the pore structure, according to the SEM images (Figure 3), the addition of β -TCP and CS particles into the collagen matrix will decrease the pore size of the scaffold. Since the pores within the freeze-dried scaffold were determined by the ice crystal formation and water sublimation [41], various factors, such as solubility, collagen concentration, freeze-drying rate, and collagen-based slurry viscosity, may affect the pore size of the freeze-dried collagen scaffold [42]. In this study, the solution solubility, collagen concentration, and freeze-drying rate were kept constant. Therefore, the slurry viscosity from the composite scaffolds may have decreased the pore size, which is attributable to the following reason: with the addition of β -TCP or CS (>30 wt%) particles, a higher force was required for the migration of water molecules in the collagen-based slurry. This resulted in a reduced size of inter-trapped ice blocks and induced smaller pores (e.g., 81 μm pore for pure collagen scaffold and 26 μm pore for collagen/ β -TCP/CS scaffold) during the freeze-drying process [42,43].

Next, investigation of the correlation between density and mechanical property was carried out. First, the standard deviations of density, as shown in Figure 8, for collagen/ β -TCP, collagen/ β -TCP/CS, and collagen/CS were 14.0%, 3.7%, and 1.0%, respectively. This result suggests that the dispersion of smaller CS particles ($\sim 10 \mu\text{m}$) is better than that of the larger β -TCP particles ($\sim 300 \mu\text{m}$). Thus, the density deviation of the collagen/CS was smaller than that of the collagen/ β -TCP composite scaffold. Moreover, for the mechanical property, several studies have demonstrated that the addition of stiff bioceramics particles (e.g., β -TCP [44,45] and CS particles [46]) has positive impacts on the compressive mechanical properties of collagen scaffolds. For example, Goodarzi et al. reported that the compressive modulus of a 66.7 wt% β -TCP-containing collagen scaffold (33.15 kPa) is higher than that (27.94 kPa) of a pure collagen scaffold. Meanwhile, a similar trend could be observed in this study. The compressive modulus values (1580–3680 kPa) of composite scaffolds are larger than that of the pure collagen scaffold (8 kPa). In summary, the addition of β -TCP or CS particles into the collagen matrix showed improvement in the mechanical properties of the composite scaffolds.

As for the degradation rate, both pore size and a materials' degradation behavior will affect the degradation behaviors of composite scaffolds. First, the correlation between the pore size and weight loss of composite scaffolds is plotted in Figure 9. It can be seen in the graph that with larger pore sizes, greater weight loss occurred, which shows a direct relationship. Second, the constants of solubility for β -TCP and CS were ($K_{SP} = 2.0 \times 10^{-29}$) and ($K_{SP} = 2.5 \times 10^{-8}$), resulting in an order of degradation speed of CS > β -TCP. In theory, the degradation rate of collagen/CS scaffolds is supposed to be higher than that of the collagen/ β -TCP scaffold. However, our degradation measurement shows a contrary result (degradation of the collagen/ β -TCP case is higher than that of the collagen/CS case), which implies that the factor of pore size dominates the degradation behavior of composite scaffolds. Based on Kothapalli et al.'s study, an inhomogeneous distribution of bioceramic HA particles in the scaffolds results in poor mechanical properties (e.g., compression modulus) [47]. In our study, the β -TCP particles were too large (300 μm) to form homogenous scaffolds, which resulted in a large deviation in bulk density (Figure 8). Therefore, the reason why the collagen/ β -TCP/CS scaffold possessed the highest density

but not the highest compressive modulus may have been the non-homogeneous distribution of β -TCP particles in the composite scaffold.

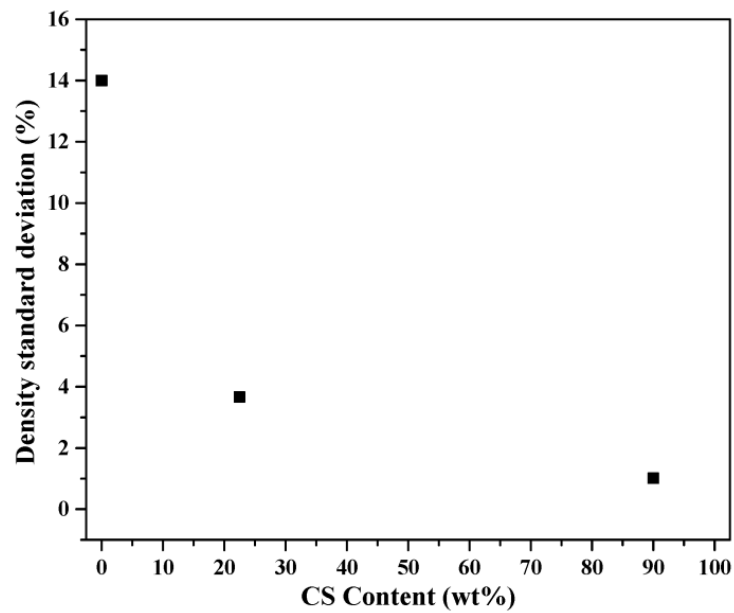


Figure 8. Density standard deviation of composite scaffolds with various CS content.

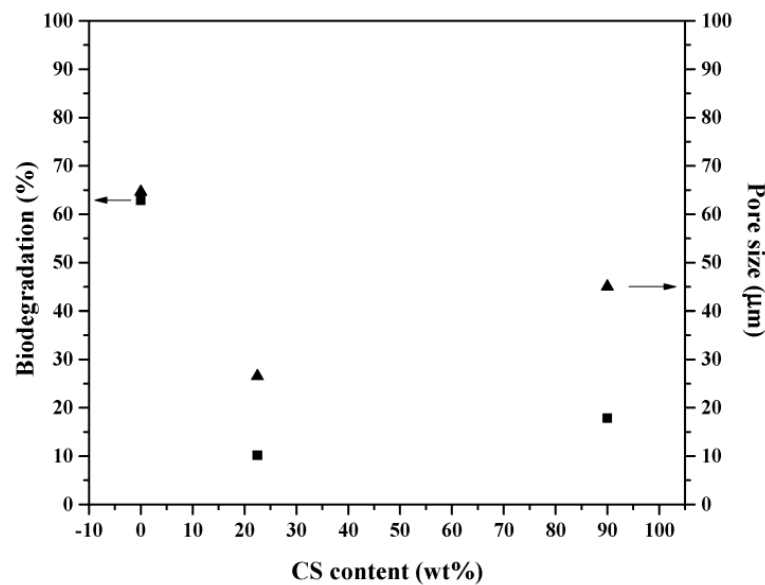


Figure 9. Correlation between biodegradation and pore size of composite scaffolds as the function of CS content.

Finally, cell viability was investigated. According to the MTT assay (see Figure 6), the results revealed that no obvious cytotoxicity could be observed for all scaffolds. In addition, several studies reported that incorporating β -TCP and CS particles into a collagen scaffold facilitated cell proliferation and differentiation after cultivating osteoblast cells incubated for 3 d [48,49]. Lopes et al. [48] reported that β -TCP/CS composite scaffolds could enhance cell attachment on the surface of composite scaffolds, which implies an excellent interaction between cells and scaffolds. These studies showed positive impacts which support our results and suggest that the addition of β -TCP and CS particles could be beneficial for future biomedical applications.

5. Conclusions

In summary, a pure collagen scaffold and collagen/ β -TCP, collagen/CS, and collagen/ β -TCP/CS composite scaffolds were successfully fabricated via the freeze-drying technique. Characterizations of morphology indicated that interconnected porous structures were present in all specimens. Meanwhile, the addition of CS or β -TCP particles showed enhancement of the compressive modulus in all composite scaffolds. In addition, scaffolds with smaller CS particles showed a homogenous distribution, which led to a smaller standard deviation of the compressive modulus, as compared to the β -TCP ones. Among these composite scaffolds, the collagen/ β -TCP composite scaffold exhibited the fastest degradation rate due to the higher solubility constant of β -TCP. Furthermore, all scaffolds showed good biocompatibility by showing no potential cytotoxicity against osteoblast cells. This study shows that collagen/ β -TCP, collagen/CS, or collagen/ β -TCP/CS composite scaffolds are potential candidates for bone tissue engineering applications.

Author Contributions: Conceptualization, S.-J.S.; methodology, H.-H.S.; formal analysis, T.Y.A., H.-H.S. and H.S.N.; data curation, T.Y.A.; writing—original draft preparation, H.S.N.; writing—review and editing, H.S.N., M.-H.W. and S.-J.S.; supervision, S.-J.S.; funding acquisition, M.-H.W. and S.-J.S. All authors have read and agreed to the published version of the manuscript.

Funding: This research and APC was funded by National Science and Technology Council of Taiwan (grant number of NSTC 108-2923-E-011-007-MY3 and NSTC 111-2221-E-011-117) and for the Taipei Medical University/National Taiwan University of Science and Technology cross-university collaboration project (under Grant TMU-NTUST-111-10).

Institutional Review Board Statement: Not applicable.

Informed Consent Statement: Not applicable.

Data Availability Statement: Not applicable.

Conflicts of Interest: The authors declare no conflict of interest.

References

1. Betz, R.R. Limitations of autograft and allograft: New synthetic solutions. *Orthopedics* **2002**, *25*, S561–S570. [[CrossRef](#)] [[PubMed](#)]
2. Brown, K.L.; Cruess, R.L. Bone and cartilage transplantation in orthopaedic surgery. *J. Bone Jt. Surg.* **1982**, *64*, 270–279. [[CrossRef](#)]
3. Younger, E.M.; Chapman, M.W. Morbidity at bone graft donor sites. *J. Orthop. Trauma* **1989**, *3*, 192–195. [[CrossRef](#)] [[PubMed](#)]
4. Arrington, E.D.; Smith, W.J.; Chambers, H.G.; Bucknell, A.L.; Davino, N.A. Complications of iliac crest bone graft harvesting. *Clin. Orthop. Relat. Res.* **1996**, *329*, 300–309. [[CrossRef](#)]
5. Damien, C.J.; Parsons, J.R. Bone graft and bone graft substitutes: A review of current technology and applications. *J. Appl. Biomater. Biomech.* **1991**, *2*, 187–208. [[CrossRef](#)]
6. Vaccaro, A.R. The role of the osteoconductive scaffold in synthetic bone graft. *Orthopedics* **2002**, *25*, 571–578. [[CrossRef](#)]
7. Jing, X.; Salick, M.R.; Cordie, T.; Mi, H.-Y.; Peng, X.-F.; Turng, L.-S. Electrospinning homogeneous nanofibrous poly (propylene carbonate)/gelatin composite scaffolds for tissue engineering. *Ind. Eng. Chem. Res.* **2014**, *53*, 9391–9400. [[CrossRef](#)]
8. O'Brien, F.J. Biomaterials & scaffolds for tissue engineering. *Mater. Today* **2011**, *14*, 88–95.
9. Winkler, T.; Sass, F.; Duda, G.; Schmidt-Bleek, K. A review of biomaterials in bone defect healing, remaining shortcomings and future opportunities for bone tissue engineering: The unsolved challenge. *Bone Jt. Res* **2018**, *7*, 232–243. [[CrossRef](#)]
10. Boyce, S.T.; Lalley, A.L. Tissue engineering of skin and regenerative medicine for wound care. *Burns Trauma* **2018**, *6*, 1–10. [[CrossRef](#)]
11. Visser, R.; Rico-Llanos, G.A.; Pulkkinen, H.; Becerra, J. Peptides for bone tissue engineering. *J. Control Release* **2016**, *244*, 122–135. [[CrossRef](#)] [[PubMed](#)]
12. Yamada, S.; Yamamoto, K.; Ikeda, T.; Yanagiguchi, K.; Hayashi, Y. Potency of fish collagen as a scaffold for regenerative medicine. *BioMed Res. Int.* **2014**, *2014*, 302932. [[CrossRef](#)]
13. Chen, Z.; Du, T.; Tang, X.; Liu, C.; Li, R.; Xu, C.; Tian, F.; Du, Z.; Wu, J. Comparison of the properties of collagen–chitosan scaffolds after γ -ray irradiation and carbodiimide cross-linking. *J. Biomater. Sci. Polym. Ed.* **2016**, *27*, 937–953. [[CrossRef](#)] [[PubMed](#)]
14. Ohan, M.P.; Weadock, K.S.; Dunn, M.G. Synergistic effects of glucose and ultraviolet irradiation on the physical properties of collagen. *J. Biomed. Mater. Res.* **2002**, *60*, 384–391. [[CrossRef](#)]
15. Sayin, E.; Rashid, R.H.; Rodríguez-Cabello, J.C.; Elsheikh, A.; Baran, E.T.; Hasirci, V. Human adipose derived stem cells are superior to human osteoblasts (HOB) in bone tissue engineering on a collagen-fibroin-ELR blend. *Bioact. Mater.* **2017**, *2*, 71–81. [[CrossRef](#)]

16. Clarke, K.; Graves, S.; Wong, A.; Triffitt, J.; Francis, M.; Czernuszka, J. Investigation into the formation and mechanical properties of a bioactive material based on collagen and calcium phosphate. *J. Mater. Sci. Mater. Med.* **1993**, *4*, 107–110. [[CrossRef](#)]
17. Dong, C.; Lv, Y. Application of collagen scaffold in tissue engineering: Recent advances and new perspectives. *Polymers* **2016**, *8*, 42. [[CrossRef](#)]
18. Donzelli, E.; Salvade, A.; Mimo, P.; Viganò, M.; Morrone, M.; Papagna, R.; Carini, F.; Zaopo, A.; Miloso, M.; Baldoni, M. Mesenchymal stem cells cultured on a collagen scaffold: In vitro osteogenic differentiation. *Arch. Oral Biol.* **2007**, *52*, 64–73. [[CrossRef](#)]
19. Mallick, M.; Are, R.P.; Babu, A.R. An overview of collagen/bioceramic and synthetic collagen for bone tissue engineering. *Materialia* **2022**, *22*, 101391. [[CrossRef](#)]
20. Boanini, E.; Gazzano, M.; Nervi, C.; Chierotti, M.R.; Rubini, K.; Gobetto, R.; Bigi, A. Strontium and zinc substitution in β -tricalcium phosphate: An X-ray diffraction, solid state NMR and ATR-FTIR study. *J. Funct. Biomater.* **2019**, *10*, 20. [[CrossRef](#)]
21. Guarino, V.; Causa, F.; Ambrosio, L. Bioactive scaffolds for bone and ligament tissue. *Expert Rev. Med. Devices* **2007**, *4*, 405–418. [[CrossRef](#)]
22. LeGeros, R.Z. Properties of osteoconductive biomaterials: Calcium phosphates. *Clin. Orthop. Relat. Res.* **2002**, *395*, 81–98. [[CrossRef](#)] [[PubMed](#)]
23. Klein, C.; Driessen, A.; De Groot, K.; Van Den Hooff, A. Biodegradation behavior of various calcium phosphate materials in bone tissue. *J. Biomed. Mater. Res.* **1983**, *17*, 769–784. [[CrossRef](#)] [[PubMed](#)]
24. Goodarzi, H.; Hashemi-Najafabadi, S.; Baheiraei, N.; Bagheri, F. Preparation and characterization of nanocomposite scaffolds (collagen/ β -TCP/SrO) for bone tissue engineering. *Tissue Eng. Regen. Med.* **2019**, *16*, 237–251. [[CrossRef](#)] [[PubMed](#)]
25. Zou, C.; Weng, W.; Deng, X.; Cheng, K.; Liu, X.; Du, P.; Shen, G.; Han, G. Preparation and characterization of porous β -tricalcium phosphate/collagen composites with an integrated structure. *Biomaterials* **2005**, *26*, 5276–5284. [[CrossRef](#)] [[PubMed](#)]
26. Wang, X.; Zhou, Y.; Xia, L.; Zhao, C.; Chen, L.; Yi, D.; Chang, J.; Huang, L.; Zheng, X.; Zhu, H. Fabrication of nano-structured calcium silicate coatings with enhanced stability, bioactivity and osteogenic and angiogenic activity. *Colloids Surf. B Biointerfaces* **2015**, *126*, 358–366. [[CrossRef](#)] [[PubMed](#)]
27. Dong, Y.; Duan, H.; Zhao, N.; Liu, X.; Ma, Y.; Shi, X. Three-dimensional printing of β -tricalcium phosphate/calcium silicate composite scaffolds for bone tissue engineering. *Bio-Design. Manufact.* **2018**, *1*, 146–156. [[CrossRef](#)]
28. Xie, Y.; Lee, K.; Wang, X.; Yoshitomi, T.; Kawazoe, N.; Yang, Y.; Chen, G. Interconnected collagen porous scaffolds prepared with sacrificial PLGA sponge templates for cartilage tissue engineering. *J. Mater. Chem. A* **2021**, *9*, 8491–8500. [[CrossRef](#)] [[PubMed](#)]
29. Liang, D.; Hsiao, B.S.; Chu, B. Functional electrospun nanofibrous scaffolds for biomedical applications. *Adv. Drug Deliv. Rev.* **2007**, *59*, 1392–1412. [[CrossRef](#)]
30. Keshaw, H.; Thapar, N.; Burns, A.J.; Mordan, N.; Knowles, J.C.; Forbes, A.; Day, R.M. Microporous collagen spheres produced via thermally induced phase separation for tissue regeneration. *Acta Biomater.* **2010**, *6*, 1158–1166. [[CrossRef](#)]
31. Mabrouk, M.; Beherei, H.H.; Das, D.B. Recent progress in the fabrication techniques of 3D scaffolds for tissue engineering. *Mater. Sci. Eng. C* **2020**, *110*, 110716. [[CrossRef](#)]
32. Thomson, R.C.; Shung, A.K.; Yaszemski, M.J.; Mikos, A.G. Polymer scaffold processing. In *Principles of Tissue Engineering*; Elsevier: Amsterdam, The Netherlands, 2000; pp. 251–262.
33. Finoli, A.; Ostrowski, N.; Schmelzer, E.; Nettleship, I.; Gerlach, J. Multiscale porous ceramic scaffolds for in vitro culturing of primary human cells. *Adv. Appl. Ceram.* **2012**, *111*, 262–268. [[CrossRef](#)]
34. Yannas, I.; Lee, E.; Orgill, D.P.; Skrabut, E.; Murphy, G.F. Synthesis and characterization of a model extracellular matrix that induces partial regeneration of adult mammalian skin. *Proc. Natl. Acad. Sci. USA* **1989**, *86*, 933–937. [[CrossRef](#)] [[PubMed](#)]
35. Sultana, N.; Wang, M. PHBV/PLLA-based composite scaffolds fabricated using an emulsion freezing/freeze-drying technique for bone tissue engineering: Surface modification and in vitro biological evaluation. *Biofabrication* **2012**, *4*, 015003. [[CrossRef](#)] [[PubMed](#)]
36. Kuo, C.-K.; Huang, H.-W.; Chen, L.-G.; Chou, Y.-J. Fabrication and characterization of freeze dried strontium-doped bioactive glasses/chitosan composite scaffolds for biomedical engineering. *J. Asian Ceram. Soc.* **2021**, *9*, 1173–1182. [[CrossRef](#)]
37. Liapis, A.I.; Bruttini, R. Freeze drying. In *Handbook of Industrial Drying*, 4th ed.; Mujumdar, A.S., Ed.; CRC Press: Boca Raton, FL, USA, 2014; pp. 309–343.
38. Wallin, R.F. A practical guide to ISO 10993: Part 1; Introduction to the standards. *Med. Device Diagn. Ind. Mag.* **1998**, *20*, 96–99.
39. Vehring, R. Pharmaceutical particle engineering via spray drying. *Pharm. Res.* **2008**, *25*, 999–1022. [[CrossRef](#)]
40. Chou, Y.-J.; Hsiao, C.-W.; Tsou, N.-T.; Wu, M.-H.; Shih, S.-J. Preparation and in vitro bioactivity of micron-sized bioactive glass particles using spray drying method. *Appl. Sci.* **2018**, *9*, 19. [[CrossRef](#)]
41. Dorazilová, J.; Muchová, J.; Šmerková, K.; Kočiová, S.; Diviš, P.; Kopel, P.; Veselý, R.; Pavliňáková, V.; Adam, V.; Vojtová, L. Synergistic effect of chitosan and selenium nanoparticles on biodegradation and antibacterial properties of collagenous scaffolds designed for infected burn wounds. *Nanomaterials* **2020**, *10*, 1971. [[CrossRef](#)]
42. Wahl, D.; Czernuszka, J. Collagen-hydroxyapatite composites for hard tissue repair. *Eur. Cell Mater.* **2006**, *11*, 43–56. [[CrossRef](#)]
43. Arabi, N.; Zamanian, A. Effect of cooling rate and gelatin concentration on the microstructural and mechanical properties of ice template gelatin scaffolds. *Appl. Biochem. Biotechnol.* **2013**, *60*, 573–579. [[CrossRef](#)] [[PubMed](#)]
44. Arahira, T.; Todo, M. Effects of proliferation and differentiation of mesenchymal stem cells on compressive mechanical behavior of collagen/ β -TCP composite scaffold. *J. Mech. Behav. Biomed. Mater.* **2014**, *39*, 218–230. [[CrossRef](#)]

45. Arahira, T.; Todo, M. Variation of mechanical behavior of β -TCP/collagen two phase composite scaffold with mesenchymal stem cell in vitro. *J. Mech. Behav. Biomed. Mater.* **2016**, *61*, 464–474. [[CrossRef](#)]
46. Lee, D.J.; Kwon, J.; Kim, Y.I.; Wang, X.; Wu, T.J.; Lee, Y.T.; Kim, S.; Miguez, P.; Ko, C.C. Effect of pore size in bone regeneration using polydopamine-laced hydroxyapatite collagen calcium silicate scaffolds fabricated by 3D mould printing technology. *Orthod. Craniofacial Res.* **2019**, *22*, 127–133. [[CrossRef](#)] [[PubMed](#)]
47. Kothapalli, C.R.; Shaw, M.T.; Wei, M. Biodegradable HA-PLA 3-D porous scaffolds: Effect of nano-sized filler content on scaffold properties. *Acta Biomater* **2005**, *1*, 653–662. [[CrossRef](#)] [[PubMed](#)]
48. Lopes, J.H.; Magalhães, J.A.; Gouveia, R.F.; Bertran, C.A.; Motisuke, M.; Camargo, S.E.A.; Trichês, E.d.S. Hierarchical structures of β -TCP/45S5 bioglass hybrid scaffolds prepared by gelcasting. *J. Mech. Behav. Biomed. Mater.* **2016**, *62*, 10–23. [[CrossRef](#)] [[PubMed](#)]
49. Chen, X.F.; Wang, Y.J.; Zhao, N.R.; Yang, C.R. Investigation on the biomimetic scaffold for bone tissue engineering based on bioglass-collagen-hyaluronic acid-phosphatidylserine. *Key Eng. Mater.* **2007**, 330–332, 939–942. [[CrossRef](#)]

Disclaimer/Publisher’s Note: The statements, opinions and data contained in all publications are solely those of the individual author(s) and contributor(s) and not of MDPI and/or the editor(s). MDPI and/or the editor(s) disclaim responsibility for any injury to people or property resulting from any ideas, methods, instructions or products referred to in the content.